Desalination and Water Treatment
www.deswater.com
doi: 10.5004/dwt.2023.29609

298 (2023) 141–154
June

Removal behavior and mechanisms of reactive dyes from aqueous streams using engineered nanocomposites of Barona marble waste

Amina Mehmood[a], Muhammad Asif Hanif[a,*], Najla AlMasoud[b], Taghrid S. Alomar[b], Muhammad Idrees Jilani[c]

[a]*Nano and Biomaterials, Department of Chemistry, University of Agriculture, Faisalabad 38040, Pakistan, emails: drmuhammadasifhanif@gmail.com (M.A. Hanif), aminamehmood88@gmail.com (A. Mehmood)*
[b]*Department of Chemistry, College of Science, Princess Nourah bint Abdulrahman University, Riyadh 11671, Saudi Arabia, emails: nsalmaoud@pnu.edu.sa (N. AlMasoud), Tsalomar@pnu.edu.sa (T.S. Alomar)*
[c]*Department of Chemistry, The University of Lahore, Lahore 53700, Pakistan, email: idreeschemistry@gmail.com*

Received 14 January 2023; Accepted 27 May 2023

ABSTRACT

The removal of dyes from wastewater has becomes a global issue since there is no penetration of sunlight into colored waters and this results in the ultimate reduction of aquatic life forms in addition to severe diseases to humans and significant problems to the environment. An attempt was made to synthesize economical and eco-friendly nanocomposites of high adsorption capacity for dye removal. For this purpose, waste material such as Barona marble was used as an adsorbent, and its adsorption properties were enhanced by treating it with sodium metasilicate, potassium ferricyanide, and their mixture. The prepared nanocomposites effectively removed Reactive red 120 and Reactive green 5 dyes by the adsorption process. The effect of different parameters such as initial dye concentration, adsorbent dosage, time, temperature, and pH was determined for adsorption process optimization. The equilibrium adsorption data were examined using the Langmuir, Freundlich, Temkin, Dubinin–Radushkevich, and Harkins–Jura isotherm models. According to the obtained results, the pseudo-first-order kinetic model best fitted to both dyes for all four composites, considering its high R^2 values ($R^2 > 0.9$). All the prepared nanocomposites were characterized by X-ray diffraction, scanning electron microscopy, and Fourier-transform infrared spectroscopy.

Keywords: Reactive dyes; Barona marble waste; Nanocomposites; Adsorption; Color water

1. Introduction

The textile industry is one of the major contributors to global water pollution. It becomes a major concern to control and manage the amount of wastewater generated by industries which is discharged into water bodies without any treatment [1,2]. Over 10,000 dyes are widely available, and more than 7×10^5 tons of azo dyes are manufactured per year. About 5%–10% of total dyes are discarded in the wastewater during treatment processes [3]. The contaminants in water are also a primary cause of life-threatening diseases that account for around 80% of all illnesses and 33% of all deaths. In Asia, 60% of childhood deaths are caused by waterborne diseases due to contaminated water [4]. Their elimination from wastewater is important because they are uncontrollable and persist in the environment [5–13]. Dyes compound keeps away radiation to enter most of the contaminated water system and lower the dissolved oxygen concentration (DO). Dyes increased the wastewater BOD (biochemical oxygen demand) [14]. Dyes are difficult to remove from wastewater using traditional wastewater treatment procedures because they do

* Corresponding author.

not degrade efficiently in natural circumstances [15]. Due to their complex nature, reactive dyes are resistant to aerobic degradation. Reactive dyes have interference effects on the aquatic environments by obstructing the penetration of sunlight into groundwater and hindering photosynthesis, are toxic to marine species and cause human genetic changes [16]. The low cost, versatility, high solubility, and water stability of reactive azo dyes have made them very attractive. Conventional methods do not affectively remove these dyes because of their high stability and complicated chemical structure [17]. Elimination of dye contaminants from wastewater by adsorption is a reliable or cost-effective process [18]. Adsorption is the most simple and cost-effective method for removing organic and inorganic contaminants from wastewater [19]. The adsorption technique is useful because of its simplicity, high efficiency, and application to a wide range of pollutants. Adsorption process controlled by the interaction between the adsorbate and adsorbent such as simple mass transfer, hydrogen bonding and weak van der wall forces.

Marble-derived compounds such as granite, agricultural or industrial wastes have been used as adsorbents due to their natural origin and low cost [20]. Because of their adsorption kinetics, lack of selectivity, and surface area, traditional adsorbents are ineffective. Due to various properties as limited intraparticle diffusion space, high surface chemistry, sorption position, high specific surface area, and variable size distribution, nano adsorbents are widely used for wastewater treatment [21]. Nano materials have wide applications in several fields [22]. Nano adsorbents including nanocomposites and activated carbon provide an active site for reactive dyes to adsorb from wastewater. Increasing particle size with increase in percentage removal largely suggests that the dye does not fully penetrate, or the dye selectively adsorb near the particle's surface layer. It is well known that adsorption is confined to the adsorbent's external surface region. As a result, the smaller particle size reduces external amount transfer resistance and helps in adsorbate penetration inside the adsorbent by the interaction with additional active sites during the adsorption process [23]. Activated carbon with reduced adsorption kinetics and decreased bulky adsorbate adsorption efficiency owing to its microporous nature, high cost, disposal issues, are hard to regenerate. So, inexpensive, active adsorbents such as marble derivative have become essential. Due to various significant adsorption and complexion capabilities, marble powder has been widely examined [24]. Marble powder is an inorganic adsorbent [25]. It is the most widely used natural stone on the planet. So, according to estimates, approximately 500 million metric tons of marble stone are extracted every year, with approximately 12 million metric tons of marble waste produced [26]. It is widely accessible, inexpensive inorganic adsorbent. For example, its effectiveness in removing methylene blue produced positive results and the treated water has no harmful effects on the environment [27].

This project aims to extract toxic dyes from wastewater using low cost Barona marble powder (waste) nanocomposite as a new moderate adsorbent and to determine its extraction efficiency for reactive dyes using the results of a variety of parameters such as adsorbent dosage, concentration, pH solution, temperature, and agitation time [28,29]. A very first approach to use for determining the adsorption behavior of Barona marble with kinetic and adsorption isotherm comparison. The prepared nano composites were BMSS (Barona modified with sodium metasilicate), BMPF (Barona modified with potassium ferricyanide), BMM (Barona was modified with a mixture of sodium metasilicate and potassium ferricyanide) and BMUM (Barona unmodified).

2. Material and methods

2.1. Materials

The Reactive green 5 and Reactive red 120 dye of high purity used during research work was purchased from the local dye industry. The absorbance of the dye's solution was measured by using a UV-Visible spectrophotometer in the range of (340–1,000 nm) to determine their maximum wavelengths. Barona marble powder was leftover collected after sawing and shaping marble in a local industry. The collected material was further grinded and sieved to attain a uniform size and stored in airtight plastic bottles.

2.2. Preparation of adsorbent nanocomposites

Fine powdered Barona marble was used to make nanocomposites (Figs. 1 and 2). The nanocomposites were prepared by the following simple procedure. 20 g of Barona marble powder was taken and further ground to obtain fine powder form by using a ceramic-based pestle and mortar. The adsorbent was divided into four equal portions of 5 g. 5 g of adsorbent remains untreated. 5 g of material were treated with a saturated solution of sodium metasilicate, 5 g were treated with a saturated solution of potassium ferricyanide, and 5 g were treated with a saturated solution of a mixture of both (sodium metasilicate and potassium ferricyanide). All these pastes were put into the crucibles and covered with aluminum foil. All these pastes were placed in the oven (WHL-25A) and fully dried at a temperature of 150°C for 2 h. After drying, the adsorbents were again ground to very fine powders. After grinding, the marble powder was washed by using deionized water to remove the color of the chemicals used and other impurities. Washing was done until the filtrate was clear (no color). After washing, the adsorbents were first

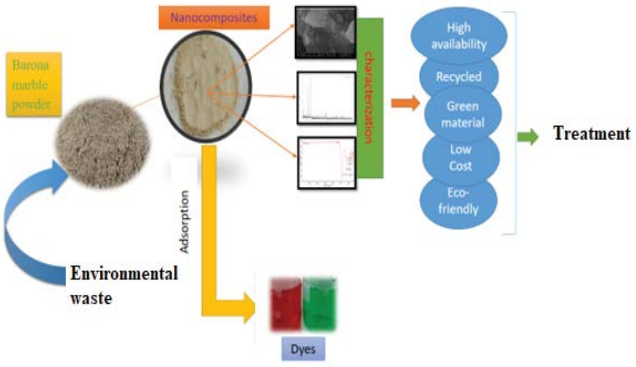

Fig. 1. Schematic representation of the study.

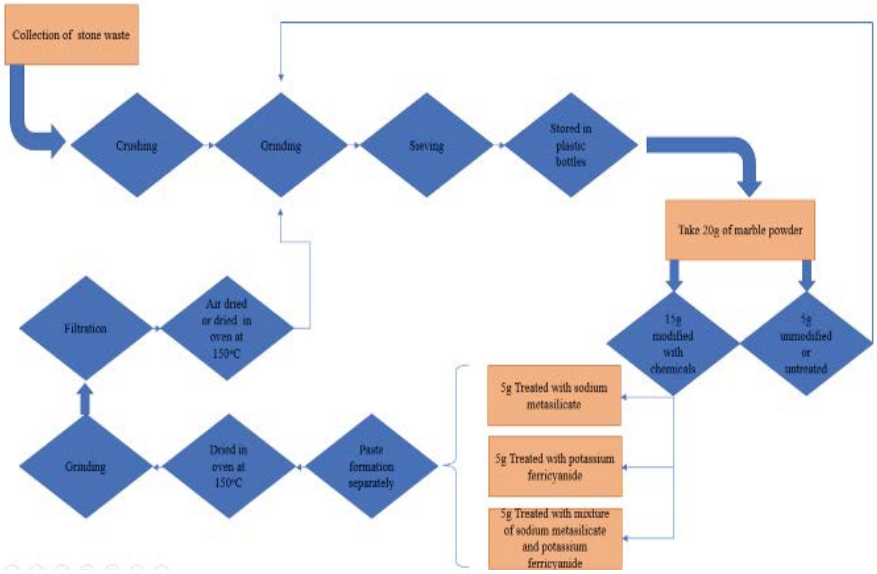

Fig. 2. Schematic representation of preparation of adsorbents nanocomposites.

air-dried and then placed in the oven at 150°C until fully dried. When the adsorbents were fully dried, they were again ground and sieved in the form of very fine powder. The prepared nano composites were BMSS (Barona modified with sodium metasilicate), BMPF, BMM and BMUM.

2.3. Adsorption process

Falcon tubes (15 mL plastic disposable test tubes), each containing 10 mL of solution (dye + adsorbent) was used to conduct adsorption experiments. Tubes were shaken for 2 h at 300 rpm on an orbital shaker (PA250/25H) [30]. The solution was then filtered using a 0.45 μL microfilter (disposable). The filtrate is then run through a 721D spectrophotometer to measure its absorbance at the λ_{max} of the dye. The solutions of 5, 10, 15, 25, 50, and 75 ppm were prepared from the stock dye solution of 100 ppm and measured their absorbance on the λ_{max} of each dye using a spectrophotometer. The standard factor was determined from standard curves and calculated by using Eq. (1).

$$\text{Standard factor} = \frac{\text{Concentration}}{\text{absorbance}} \tag{1}$$

The following Eq. (2) was used to determine the removal efficiency and adsorption capacity of all adsorbents.

$$\%\text{age removal} = \frac{C_o - C_e}{C_o} \times 100 \tag{2}$$

The effect of experimental parameters on adsorption was determined with different dye concentrations (5, 10, 15, 25, 50, and 75 ppm) and varying adsorbent dose (0.005, 0.01, 0.02, 0.03, and 0.04 g). The pH adjustment was made using 0.1 N HCl and 0.1 N NaOH solution from 5 to 10 pH before adding the adsorbent in order to test the impact of pH on a 50 ppm dye solution. The effect of time and temperature on adsorption was determined at 30°C, 40°C, 50°C, 60°C, and 70°C for 15, 30, 60, 120, and 240 min. The removal efficiency was determined by using Eq. (3).

$$q = \frac{C_o - C_e}{m \times V} \tag{3}$$

where C_o = initial dye concentration, C_e = dye concentration after treatment, m = mass of adsorbent, V = volume of dye solution.

2.4. Adsorption isotherms

Adsorption equilibrium determines the relationship between the specific amounts of solute adsorbed by the adsorbent and optimizes the solute concentration in the liquid phase. They are crucial to the design of an adsorption process because they explain how an adsorbate interacts with an adsorbent [31]. In this research work, the adsorption process was optimized using some common equilibrium isotherm models, including Harkins–Jura isotherm, Dubinin–Radushkevich isotherm, Freundlich isotherm, Temkin isotherm, and Langmuir isotherm.

The Harkins–Jura model depicts multilayer adsorption as well as the occurrence of an uneven distribution of adsorbent pore sizes. The Harkins–Jura model can be determined by Eq. (4).

$$\frac{1}{q_e^2} = \frac{B}{A}\left(\frac{1}{A}\right)\log C_e \tag{4}$$

where A and B are the Harkins–Jura constants.

A uniform surface or a constant adsorption potential is not presupposed by the Dubinin–Radushkevich isotherm model. To discriminate between physical and chemical adsorption processes by mean free energy value, a gaussian energy distribution onto a heterogeneous surface is typically used:

$$\ln q_e = q_e - \beta\varepsilon^2 \tag{5}$$

Adsorption potential (ε) can be calculated as:

$$\varepsilon = RT\ln\left(1+\frac{1}{C_e}\right) \tag{6}$$

Mean energy (E) (kJ/mol) for the transfer of sorbate from solution calculated by the equation.

$$E = \frac{1}{(2B)^{\frac{1}{2}}} \tag{7}$$

An exponential distribution of active sites with various energies indicates multilayer adsorption on a heterogeneous surface by Freundlich isotherm. It is described by the following equation:

$$\ln q_e = \left(\frac{1}{n}\right)\ln C_e + \ln k_f \tag{8}$$

Temkin isotherm describes the uniform binding energies of adsorbate molecules on adsorbent to maximum binding energies. Its linear form is defined as:

$$q_e = B\ln A_t + B\ln C_e \tag{9}$$

Langmuir isotherm describes without any interactions in the adsorbed molecules, single-layer adsorption on a homogeneous surface with a limited number of energetically comparable locations expressed by the following equation.

$$\frac{C_e}{Q_e} = \frac{1}{Q^0 k_t} + \frac{C_e}{Q^0} \tag{10}$$

2.5. Kinetic models

Adsorption pathways and adoption mechanisms were also revealed by kinetic models. Understanding the properties of the adsorption processes by pseudo-first-order and pseudo-second-order models are represented by the following equations. Pseudo-first-order based on adsorption capacity (q–q_t) and can be expressed by the equation.

$$\log\left(q_e - q_t\right) = \left[\log q_e - \left\{\frac{k_1 \mathrm{ad}_5 t}{2.303}\right\}\right] \tag{11}$$

where q_e and q_t is amount of adsorbate adsorbed in equilibrium in time t, and $k_{1,\mathrm{ads}}$ is the pseudo-first-order rate constant (1/min).

Pseudo-second-order determines the percentage of available adsorption sites (q) that drive the process. It can also be expressed as:

$$\frac{t}{q} = \frac{1}{k_{2\mathrm{ads}} q_e^2} + \frac{t}{q_t} \tag{12}$$

where $k_{2,\mathrm{ads}}$ is the pseudo-second-order rate constant (g/mg·min) and q_e^2 initial rate constant (mg/g·min) [32].

3. Results and discussions

3.1. Spectrophotometric analysis

The spectrophotometric analysis method is the most useful analytical tool to find the concentration of a given sample. A UV-visible spectrophotometer was used to find the wavelength, at which the dye absorbed maximum light (Fig. 3) [33]. The Reactive red 120 and Reactive green 5 dye solution was scanned through 340–1,000 nm. The solution of Reactive red 120 showed maximum absorbance at 515 nm. The solution of Reactive green 5 dye shows maximum absorbance at 668 nm. For drawing standard curves, 5, 10, 15, 25, 50, 75 and 100 ppm solutions were prepared. Both dyes have shown different absorptions curves through 340–1,000 nm [34]. The linear equation for standard curves of Reactive red 120 dye and for Reactive green 5 dye were $Y = 0.0204x + 0.0141$ ($R^2 = 0.9992$), and $Y = 0.0097x + 0.0271$ ($R^2 = 0.9989$), respectively.

3.2. Optimization of process parameters

Dyes were treated with different nanocomposites including BMSS, BMPF, BMM, and untreated or BMUM. The optimized parameters during the present study were pH, dose, temperature, contact time, and initial concentration. Absorbance of each dye solution was measured at maximum wavelength by using a spectrophotometer [35]. Initial concentration of dye was optimized in the range of 5–50 ppm. Maximum adsorption of Reactive red 120 dye and Reactive green 5 dye was recorded at 50 ppm for all

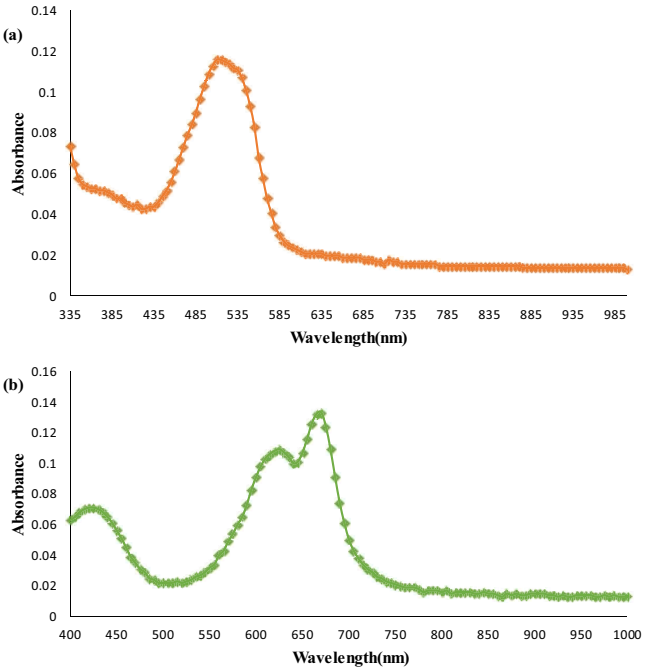

Fig. 3. The determination of λ_{max} for (a) Reactive red 120 dye and (b) Reactive green 5.

the four BMUM, BMSS, BMPF, BMM composites (Fig. 4). All these four adsorbents were able to efficiently remove both dyes having a 50 ppm concentration [36]. It may be due to resistance in dye ions uptake and decreased as the concentration of dye increased, resulting in increased driving force due to an increase in active sites on the absorbent surface [37] causing an effective collision between dye solution and adsorbent surface. Reactive red 120 dye and Reactive green 5 dye showed maximum removal efficiency at 50 ppm of dye solution by using 0.005 g for all four composites after adsorption. The reason is that the adsorbent has limited adsorption sites and further increase in the adsorbent does not affect the removal efficiency [38]. Usually, adsorption capacity and percentage removal increase with the increase in adsorbent dose. The maximum adsorption was obtained for the adsorbent dose of 0.005 g. It was observed from graphs that adsorption capacity decreased with an increase in adsorbent dose from 0.005 g to 0.04 g. An increase in the adsorption with adsorbent dose can be attributed to increased adsorbent surface area and the availability of more adsorption sites. But unit adsorption decreased with an increase in the adsorbent dose [39]. This may be attributed to overlapping or aggregation of adsorption sites at a higher dose resulting in a decrease in the total adsorbent surface area available. Therefore 0.005 g was considered as an optimum dose as all the four adsorbents have shown maximum uptake at this dose when other parameters were set constant (contact time: 2 h, shaking speed: 300 rpm, initial dye concentration: 50 ppm 7 pH).

The contact time was optimized at 15, 30, 60, 120, and 240 min at different temperatures 30°C, 40°C, 50°C, 60°C, and 70°C (Figs. 5–7). Different dyes showed different removal efficiency [40]. Reactive red 120 dye and Reactive green 5 dye solution showed maximum adsorption or removal efficiency at 240 min at all studied temperatures using BMUM, BMSS, BMPF and BMM composites. By increasing the contact time between adsorbent and the adsorbate, the removal percentage increases till reaching the equilibrium (when the removal percentage is almost constant). From the results, it can be concluded that maximum adsorption can be obtained with a maximum contact time of 240 min.

For Reactive red 120, the maximum removal capacity was obtained for BMSS, BMUM, BMPF and BMM at 60°C which refers to endothermic adsorption process. For Reactive green 5 dye maximum removal efficiency occurred for BMSS, BMUM, BMPF and BMM at 70°C which also refers to endothermic adsorption process. On increasing solution temperature of adsorbent and adsorbate, the removal percentage was increased in all cases. The pH at which the adsorbents give maximum removal efficiency was optimized at 5, 6, 7, 8, 9, and 10 pH. The pH of the solution has a significant impact on the uptake of contaminants since it determines the surface charge of the adsorbent, the degree of optimization, and the speciation of the adsorbent. As the surface of adsorbents was negatively charged at low pH in acidic medium, it would increase adsorption of positively charged ions in the solution which could occupy the negatively charged adsorption sites thus decreasing the removal efficiency of dye. Therefore, maximum dye

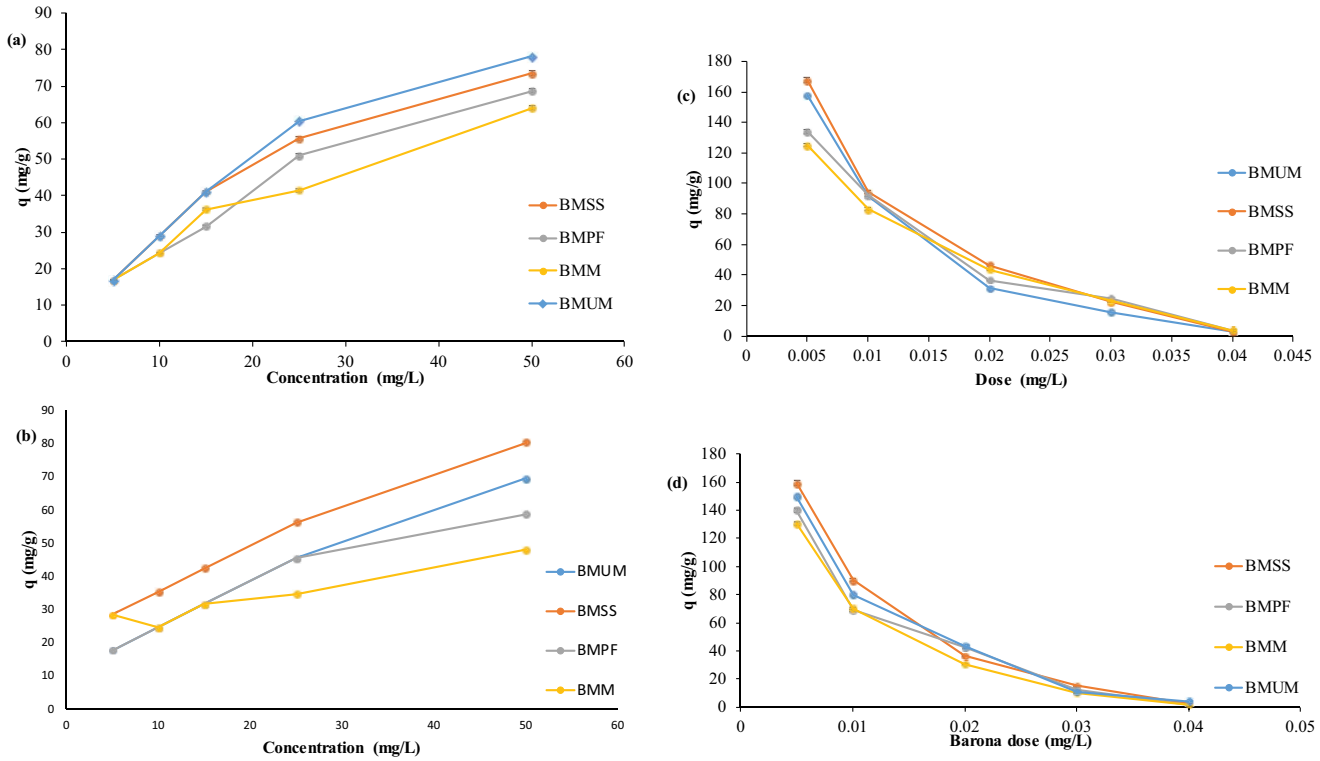

Fig. 4. Optimization of process parameters (a) initial dye concentration for Reactive red 120 dye removal, (b) initial dye concentration for Reactive green 5, (c) initial composite dose for Reactive red 120 dye removal and (d) initial composite dose for Reactive green 5.

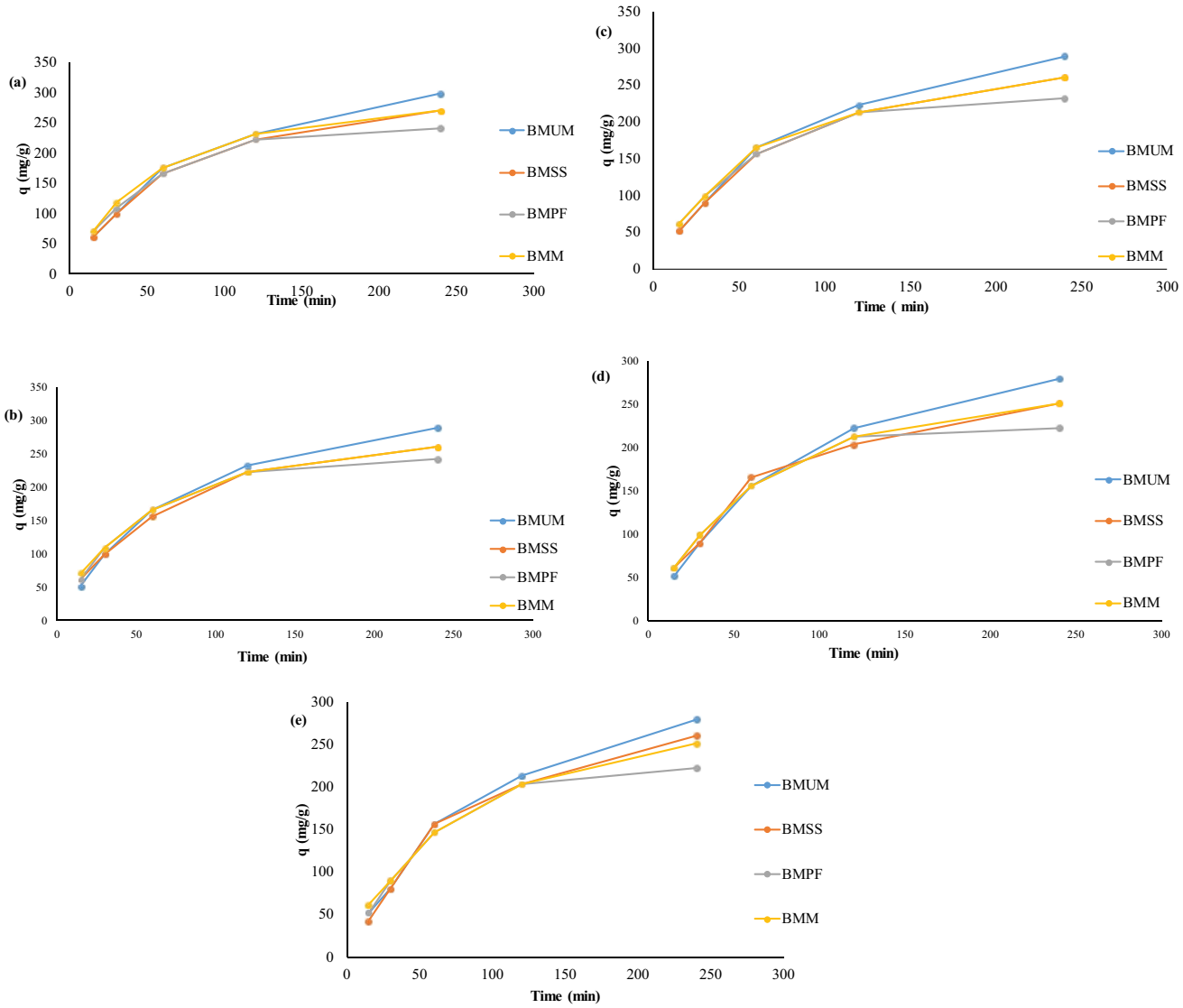

Fig. 5. Optimization of adsorption time for Reactive red 120 dye at (a) 30°C, (b) 40°C, (c) 50°C, (d) 60°C and (e) 70°C.

removal efficiency usually observed at (weak) acidic or neutral pH values [41]. The pH of all dye's solution was adjusted to different values by adding the required amount of 1 N solution of sodium hydroxide and nitric acid solution. It was observed from graphs that for Reactive red 120 dye all four BMUM, BMSS, BMPF and BMM shows maximum adsorption capacity at pH 5 at a constant contact time of 2 h, 300 rpm, 50 ppm dye solution and 0.005 g dose. For Reactive green 5 dye all the four BMUM, BMSS, BMPF and BMM have shown maximum adsorption capacity at pH 7 at a constant contact time of 2 h, 300 rpm, 50 ppm dye solution and 0.005 g dose. Higher pH favors adsorption of negatively charged species and lower pH favors adsorption of positively charged species. The higher removal at low pH is due to protonation of surface functional group which increases the attraction of adsorbent for dye anions. The adsorption decreases due to deprotonating of surface functional group at higher pH reduced the electrostatic interaction between dye ion and active binding sites [42].

3.3. Isothermal and kinetic modeling

Isotherms explains the interaction of adsorbate and adsorbent. At equilibrium, the isotherm establishes a connection between the amount of dye adsorbed on the solid phase and the concentration of dye in solution. In this study, the equilibrium adsorption data were examined using the Langmuir, Freundlich, Temkin, Dubinin–Radushkevich, and Harkins–Jura isotherm models. According to the results dyes adsorption on all nanocomposites was fitted best to Freundlich isotherms (Table 1). Freundlich model represents multilayer phenomenon and non-distinguishable distribution of the binding energies present over many exchanging sites on the surface of adsorbent. Freundlich constant K_f indicates adsorption capacity of the adsorbent. The greater K_f value, greater the adsorption capacity [31]. Magnitude of n represents the measure of favorability for adsorption. If n is equal to unity, then adsorption is linear. Moreover, n above unity represents favorable and physical adsorption.

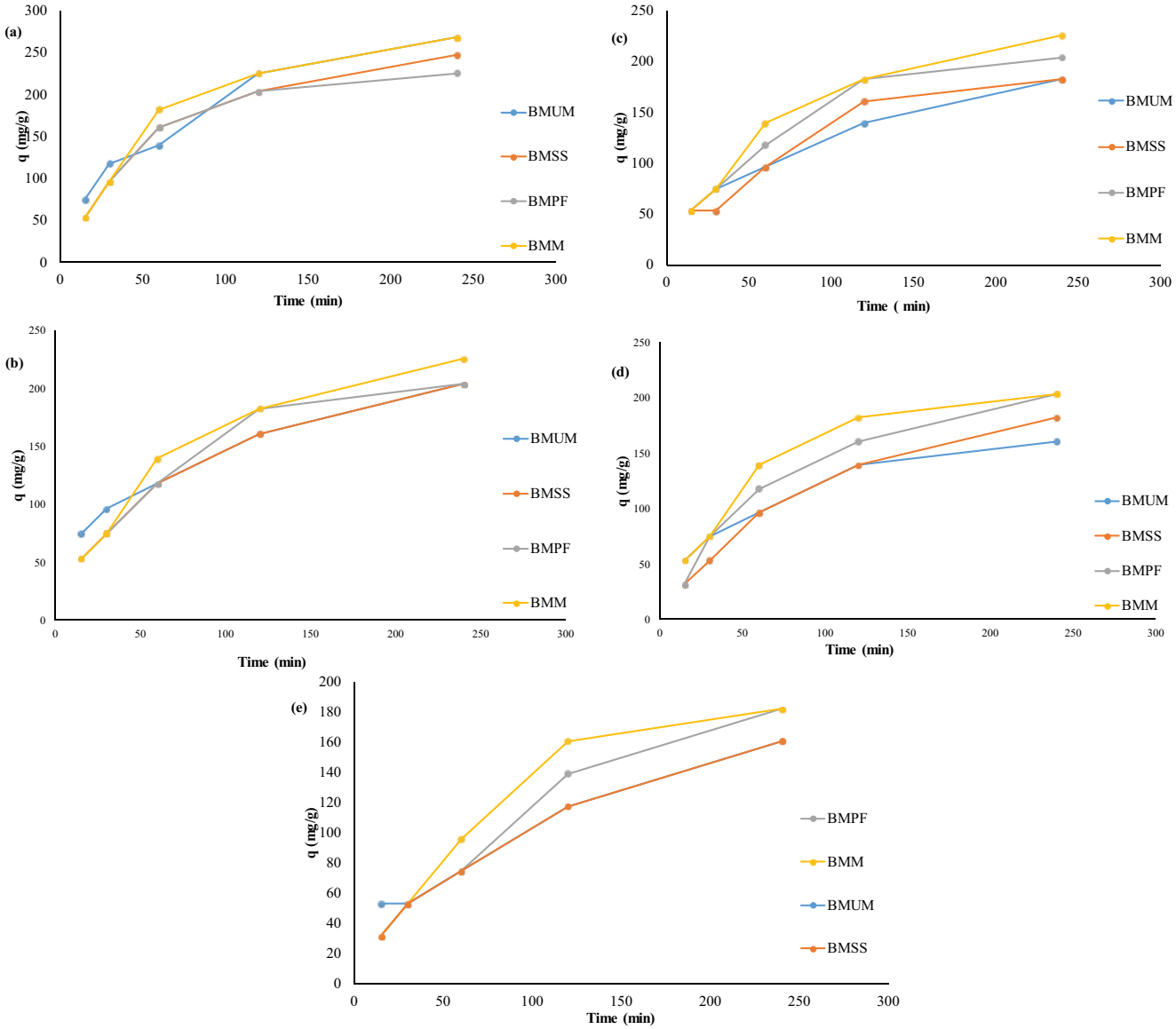

Fig. 6. Optimization of adsorption time for Reactive green 5 dye at (a) 30°C, (b) 40°C, (c) 50°C, (d) 60°C and (e) 70°C.

Adsorption kinetics models are used to explain how adsorption mechanism control chemical reaction and mass transfer. Models' conformity was evaluated using the linear regression coefficient (R^2) values. It compares experimental equilibrium adsorption capacity (q_e, exp) and theoretical values (q_e, cal) calculated from the kinetic models. According to the obtained results, pseudo-first-order kinetic model was best fitted to both dyes for BMUM, BMSS, BMPF, BMM composites, considering its high R^2 values ($R^2 > 0.9$) and close agreement between estimated values of adsorption capacities (q_e) and experimental values (q_e^{exp}) (Table 2).

The comparison of various adsorbent gives idea about their applications for dye removal [43–46]. A comparison of adsorbent's maximum adsorption capacities (mg/g) of dyes removal carried out for Reactive red 120 and Reactive green 5 in this study with the different adsorbent materials reported in the previous literature as shown in Table 3. The Barona marble nanocomposites (waste) have shown higher adsorption capacities as compared to the other adsorbents.

3.4. Characterization

The X-ray diffraction (XRD) analysis was used for characterization of Barona marble waste nanocomposites at 2θ in the range of 20°–80° at a speed of deg/min (Fig. 8). XRD analysis indicated the presence of silicate minerals in the used nanocomposites. Fourier-transform infrared (FTIR) spectra of BMUM and BMSS composites showed a wide and shoulder adsorption band attributed to Si–O stretching at 1,0006 cm^{-1}. The distinguishable peak at 1,410 cm^{-1} represents the asymmetric stretching vibrational frequency of carbonate ion while peak at 711.9 cm^{-1} due to symmetric vibrations of Ca–O bond of $CaCO_3$ in Barona marble

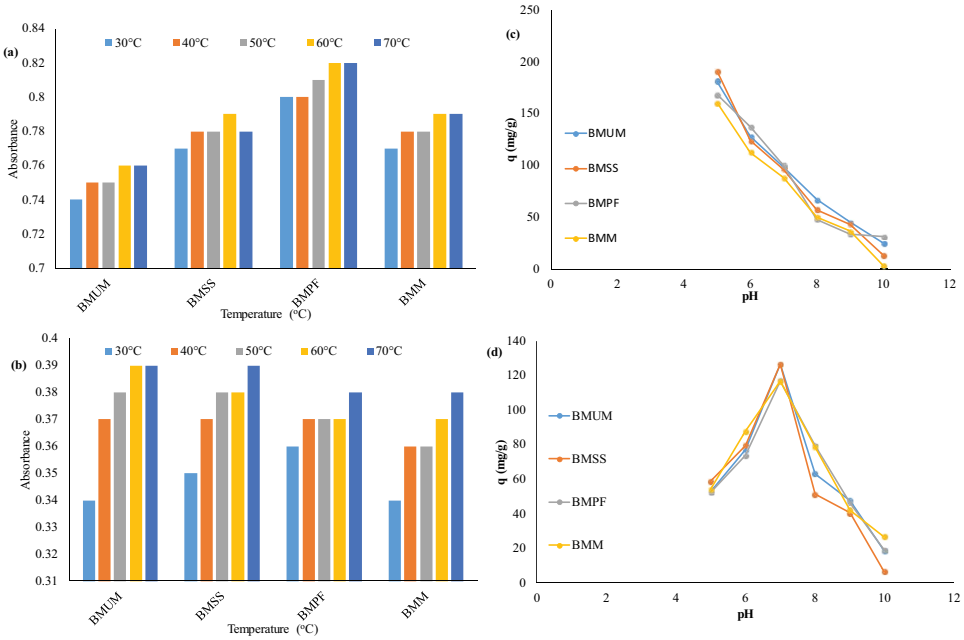

Fig. 7. Optimization of process parameters (a) temperature for Reactive red 120 dye removal, (b) temperature for Reactive green 5, (c) pH for Reactive red 120 dye removal and (d) pH for Reactive green 5.

Table 1
Comparison of different isothermal models for dye adsorption

Dyes names		Reactive red 120 dye				Reactive green 5 dye			
Adsorbents		BMUM	BMSS	BMPF	BMM	BMUM	BMSS	BMPF	BMM
Isotherms									
Harkins–Jura isotherm	A	344.8275	357.1428	333.3333	344.8275	370.3703	1,111.111	384.6153	1,428.571
	B	1.4482	1.4999	1.5333	1.5517	1.5555	1.6667	1.5769	2.4285
	R^2	0.7605	0.7554	0.8878	0.8488	0.9179	0.9844	0.8992	0.5593
	q_{max} (cal) (mg/g)	10.5923	10.6819	10.2575	10.3949	10.7762	18.3787	10.9266	18.5257
	q_{max} (exp)	78.2038	73.4645	68.7253	63.986	69.6722	80.4304	58.914	48.1558
Temkin isotherm	A_t (L/g)	0.5164	0.5711	0.5094	0.6266	0.5479	1.6131	0.7297	18.5255
	B	25.237	22.799	21.165	18.033	20.073	17.246	16.399	6.2782
	R^2	0.983	0.992	0.9388	0.9455	0.9199	0.8881	0.9605	0.6417
	q_{max} (cal) (mg/g)	77.7602	72.7991	65.3954	59.6482	63.4368	72.6892	56.9302	43.392
	q_{max} (exp)	78.2038	73.4645	68.7253	63.986	69.6722	80.4304	58.914	48.1558
Freundlich isotherm	q_{max} (cal) (mg/g)	87.9542	81.6724	70.714	64.0173	67.1226	74.4353	60.7472	41.6499
	q_{max} (exp)	78.2038	73.4645	68.7253	63.986	69.6722	80.4304	58.914	48.1558
	R^2	0.9728	0.9725	0.9799	0.9775	0.9889	0.9588	0.9876	0.6354
	K_f (L/mg)	8.608	9.1102	8.0615	9.082	8.8392	19.8737	9.8887	21.3873
	N	1.61	1.7111	1.7334	1.9331	1.8556	2.8296	2.0859	5.7175
Langmuir isotherm	K_L (L/mg)	0.0504	0.05758	0.0452	0.0578	0.0461	0.0973	0.07	0.1492
	R^2	0.991	0.998	0.9437	0.9519	0.9274	0.9486	0.9788	0.9558
	q_{max} (exp)	116.279	104.1666	103.0927	86.2068	101.01	96.1538	76.923	52.6315
	q_{max} (exp)	78.2038	73.4645	68.7253	63.986	69.6722	80.4304	58.914	48.1558
Dubinin–Radushkevich	E (kJ/mol)	408.2482	408.2482	500	500	500	845.1542	500	1,581.1388
	β (mol²/J²)	3×10^{-6}	3×10^{-6}	2×10^{-6}	2×10^{-6}	2×10^{-6}	7×10^{-7}	2×10^{-6}	2×10^{-7}
	R^2	0.8073	0.8265	0.6617	0.7175	0.6289	0.5251	0.6868	0.1492
	q^o (exp)	78.2038	73.4645	68.7253	63.986	69.6722	80.4304	58.914	48.1558
	q^o (cal) (mg/g)	57.0712	54.5708	45.7961	43.8774	44.3405	53.7637	42.1527	34.4669

Table 2
Comparison of pseudo-first-order kinetics and pseudo-second-order kinetics models for dye adsorption

Dyes	Adsorbents	Pseudo-first-order kinetic model				Pseudo-second-order kinetic model			
		q_e (mg/g) cal	q_e (mg/g) exp	R^2	$k_{1,ads}$	q_e (mg/g) cal	q_e (mg/g) exp	R^2	$k_{2,ads}$
Reactive red 120 dye					30°C				
	BMUM	278.6121	298.586	0.9906	0.0122	400	298.586	0.9968	0.00002
	BMSS	255.7996	270.151	0.9978	0.0142	357.1428	270.151	0.9987	0.00003
	BMPF	247.5711	241.715	0.996	0.0211	294.1176	241.715	0.9967	0.00007
	BMM	246.3769	270.151	0.9994	0.0156	333.3333	270.151	0.9998	0.00005
					40°C				
	BMUM	285.2331	289.108	0.999	0.0135	400	289.108	0.9958	0.00002
	BMSS	258.9405	260.672	0.9983	0.0158	333.3333	260.672	0.9981	0.00004
	BMPF	255.8558	241.715	0.9977	0.0214	294.1176	241.715	0.9944	0.00006
	BMM	239.1663	260.672	1	0.0154	322.5806	260.672	0.9993	0.00005
					50°C				
	BMUM	278.6121	289.108	0.9906	0.0122	416.6667	289.108	0.9943	0.00002
	BMSS	255.7996	260.672	0.9978	0.0142	357.1428	260.672	0.9966	0.00003
	BMPF	247.5711	232.236	0.996	0.0211	285.7142	232.236	0.9951	0.00006
	BMM	236.9736	260.672	0.9905	0.0138	333.3333	260.672	0.9985	0.00004
					60°C				
	BMUM	278.2274	279.629	0.9995	0.0133	400	279.629	0.9978	0.00002
	BMSS	224.8536	251.193	0.9707	0.0133	322.5806	251.193	0.9931	0.00004
	BMPF	276.8216	222.758	0.9855	0.0274	270.2702	222.758	0.9917	0.00007
	BMM	239.1663	251.193	1	0.0154	322.5806	251.193	0.9992	0.00004
					70°C				
	BMUM	271.7690	279.629	0.9911	0.0119	400	279.629	0.9895	0.00002
	BMSS	255.1526	260.6719	0.9821	0.0128	384.6153	260.6719	0.9817	0.00003
	BMPF	247.5711	222.7577	0.996	0.0211	285.7142	222.7577	0.9916	0.00005
	BMM	234.8551	251.1934	0.9992	0.0133	322.5806	251.1934	0.9969	0.00004
Reactive green 5 dye					30°C				
	BMUM	248.4848	268.443	0.9639	0.0140	333.3333	268.443	0.9808	0.00004
	BMSS	227.5621	246.926	0.986	0.0142	322.5806	246.926	0.996	0.00004
	BMPF	228.2443	225.41	0.9975	0.0198	285.7142	225.41	0.991	0.00006
	BMM	258.5830	268.443	0.9754	0.0154	357.1428	268.443	0.9852	0.00003
					40°C				
	BMUM	151.3561	203.894	0.9937	0.0103	238.0925	203.894	0.9833	0.00008
	BMSS	181.3844	203.894	0.9989	0.0119	256.4102	203.894	0.9944	0.00005
	BMPF	223.9752	203.894	0.9787	0.0188	263.1578	203.894	0.9887	0.00005
	BMM	211.7873	225.41	0.9891	0.0135	294.1176	225.41	0.9914	0.00004
					50°C				
	BMUM	151.3561	182.3772	0.9937	0.0103	227.2727	182.3772	0.9802	0.00006
	BMSS	203.9388	182.3772	0.9553	0.0179	243.9024	182.3772	0.945	0.00005
	BMPF	223.9752	203.8936	0.9787	0.0188	263.1578	203.8936	0.9887	0.00005
	BMM	211.7873	225.41	0.9891	0.0135	294.1176	225.41	0.9914	0.00004

Table 2 (Continued)

Table 2

Dyes	Adsorbents	Pseudo-first-order kinetic model				Pseudo-second-order kinetic model			
		q_e (mg/g) cal	q_e (mg/g) exp	R^2	$k_{1,ads}$	q_e (mg/g) cal	q_e (mg/g) exp	R^2	$k_{2,ads}$
Reactive green 5 dye				60°C					
	BMUM	141.2212	160.8608	0.9847	0.0151	192.3076	160.8608	0.9934	0.0001
	BMSS	181.3844	182.3772	0.9989	0.0119	270.2702	182.3772	0.9969	0.00003
	BMPF	196.7433	203.8936	0.9923	0.0128	294.1176	203.8936	0.9755	0.00003
	BMM	210.4262	203.8936	0.9954	0.0191	256.4102	203.8936	0.9887	0.00006
				70°C					
	BMUM	135.4565	160.861	0.9609	0.0092	204.0816	160.861	0.9364	0.00006
	BMSS	151.3561	160.861	0.9937	0.0103	227.2727	160.861	0.983	0.00004
	BMPF	190.4144	182.377	0.9703	0.0119	285.7142	182.377	0.9581	0.00002
	BMM	223.9752	182.377	0.9787	0.0064	277.7778	182.377	0.9708	0.00003

Table 3
Comparison of maximum adsorption capacities (mg/g) of reactive dyes on Barona marble nanocomposites (waste) with other adsorbents

Adsorbents	Dye/Compound	Adsorption capacity	References
Peat	Basic blue 9	15.70 mg/g	[5]
Furnace slag	Acid blue 29	12.85 mg/g	
Bentonite clay	Acid red 91	161.1 mg/g	
Fly ash	Disperse red 1	140.1 mg/g	
Nano-MgO	Reactive red (RR 198)	125 mg/g	[14]
	Reactive blue (RB 19)	166.7 mg/g	
Activated carbon derived from poplar wood	Acid red (AR 18)	29.41 mg/g	[17]
Marble dust	Methylene blue (MB)	16.36 mg/g	[27]
Cellolignin	Methylene blue (MB)	15.85 mg/g	[30]
Activated sludge	Reactive blue 2 (RB 2) and Reactive yellow 2 (RY 2)	107.1 mg/g 123.5 mg/g	[35]
Eggshell	Reactive yellow 205 (RY 205)	0.2569 mg/g	[36]
Raw marble powder	Reactive red 195	99 mg/g	[41]
Sorel's cement	Reactive yellow 145 (RY 145), Reactive red 194 (RR 194), Reactive blue B (RB-B)	120.89 mg/g	[42]
Na-X zeolite	Reactive black 5 (RB 5)	25.3 mg/g	[43]
Na-X zeolite	Brilliant green (BG)	24.13 mg/g	[43]
Mango seeds activated carbon (MSAC)	Doxorubicin hydrochloride (DOX)	0.25 mmol/g	[46]
Zeolitic imidazolate framework-7 (ZIF-7)	Methylene blue (MB)	2.42 mmol/g	[44]
BMUM	Reactive red 120 (RR 120)	298.5 mg/g	Present study
BMSS		270.1 mg/g	
BMPF		241.7 mg/g	
BMM		270.1 mg/g	
BMUM	Reactive green 5 (RG 5)	268.4 mg/g	
BMSS		246.9 mg/g	
BMPF		225.4 mg/g	
BMM		268.4 mg/g	

powder. Appearances of peak near 874 cm^{-1} for calcium carbonate and 777.1 and 795.9 cm^{-1} shows the presence of silicates in the material. FTIR pattern for the nanocomposites is shown in Fig. 8. Scanning electron microscope with TLD and ETD analysis were used to study the morphology and surface of BMUM and BMSS nanocomposites. At different magnifications, the scanning electron micrographs suggested that BMUM showed spherical and sub spherical

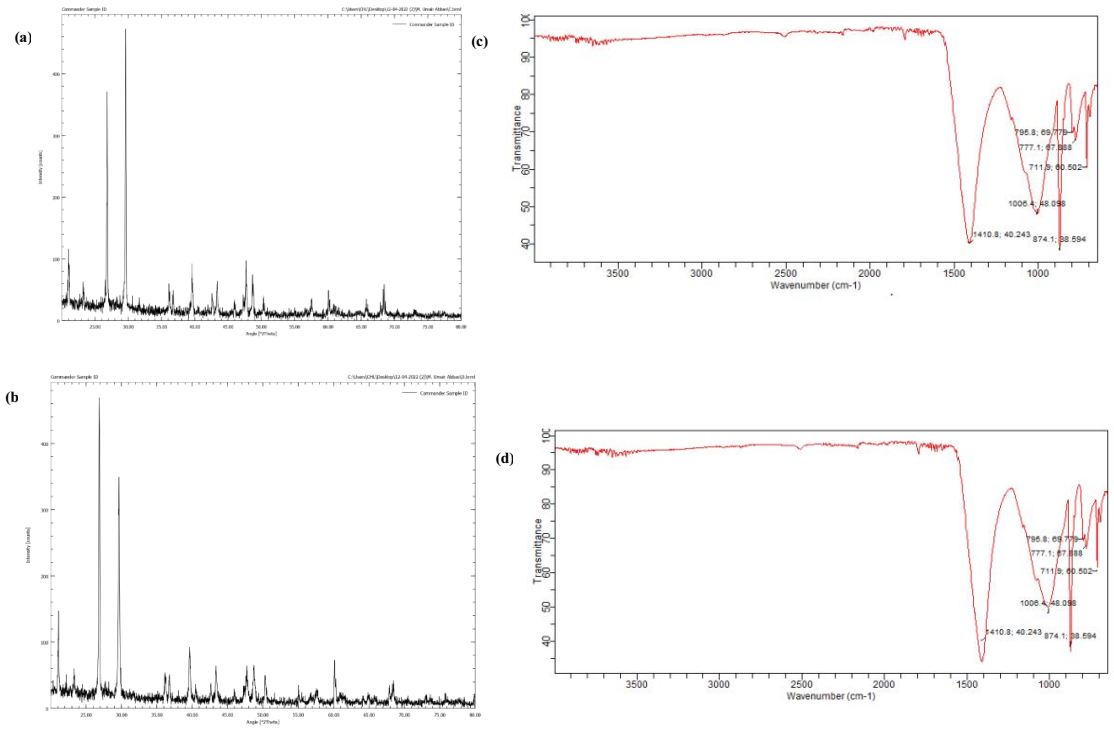

Fig. 8. Characterization of Barona marble nanocomposites (a) X-ray diffraction spectra of Barona unmodified, (b) X-ray diffraction spectra of Barona modified with sodium metasilicate, (c) Fourier-transform infrared spectra of Barona unmodified and (d) Fourier-transform infrared spectra of Barona modified with sodium metasilicate.

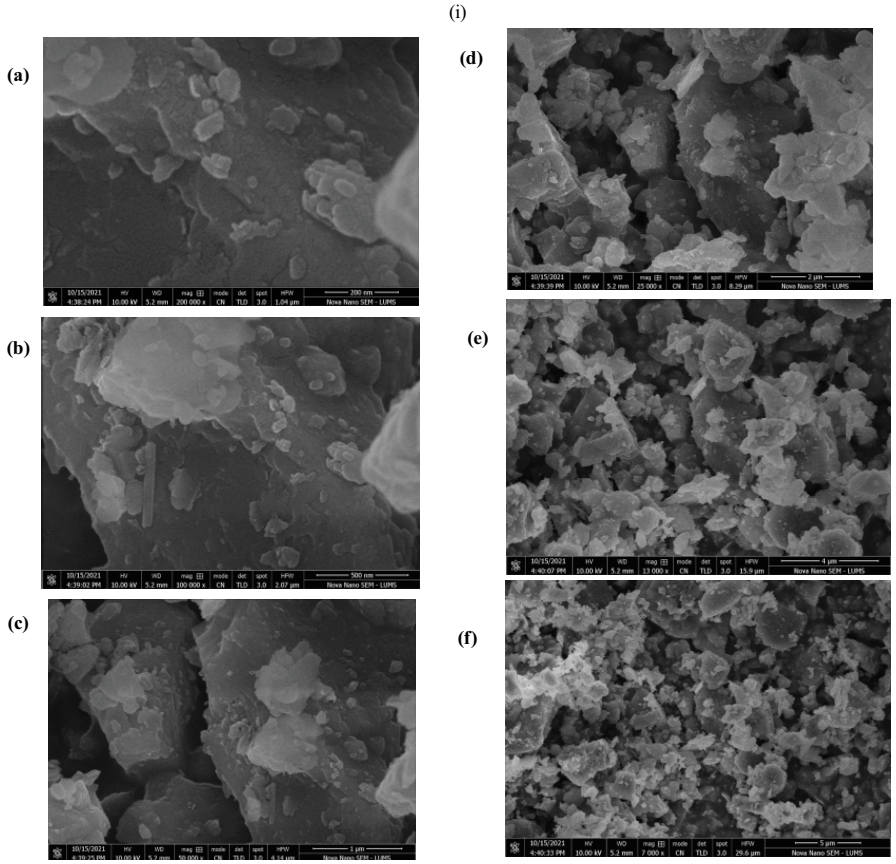

Fig. 9. (Continued)

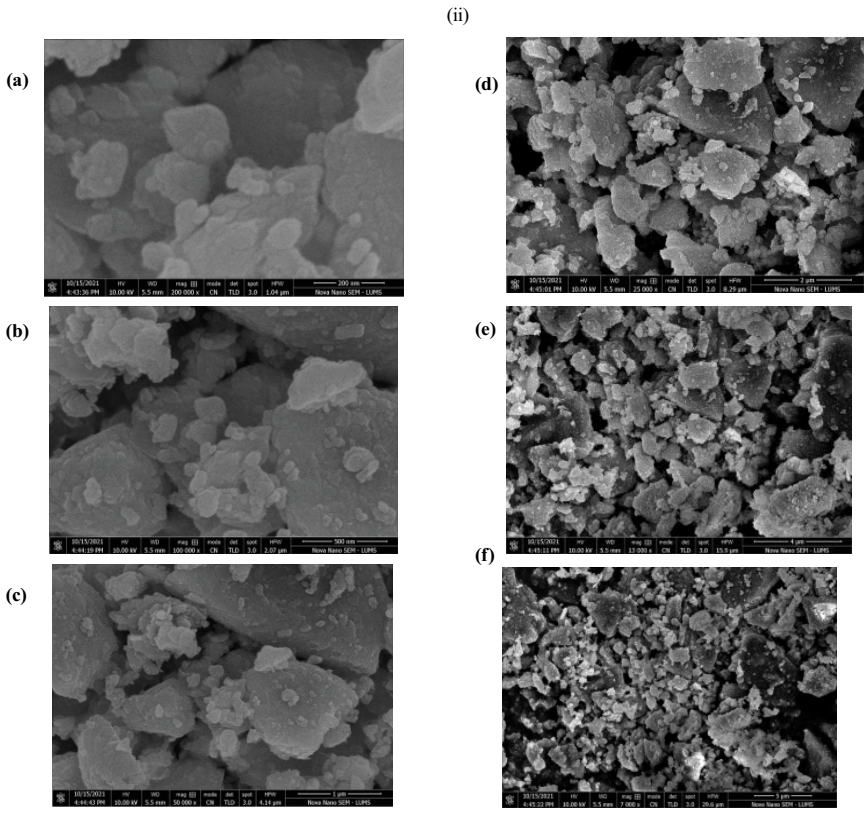

Fig. 9. Scanning electron micrographs of nanocomposites at various resolutions (i) Barona unmodified and (ii) Barona modified with sodium metasilicate.

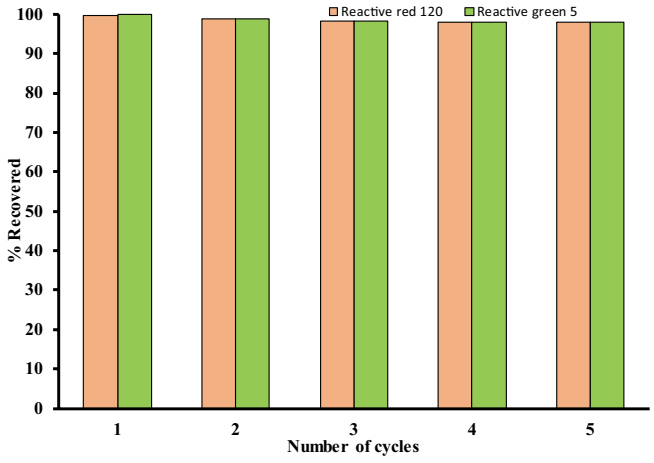

Fig. 10. Reusability of studies of adsorbent.

and cylindrical shapes of particles (as nanotube formation) with less pore size and BMSS shows irregular shapes of different particle size with increase pore size due to modification to facilitate adsorption. The morphological study of both adsorbents at different magnifications given separately in Fig. 9. The characterization results clearly indicated that prepared nanocomposites have better surface and adsorption properties than the pure material.

3.5. Study of desorption and reusability of adsorbents

In this context, the reusability of marble having maximum adsorption capacity was investigated by using CH_3OH as an eluent for up to five consecutive cycles (Fig. 10). The amount of dye present in the solution was checked to calculate the removal efficiency after each cycle. It can be noted from results that dye uptake capacity of adsorbent was slightly affected after each cycle. Thus, this adsorbent can be effectively used for dye removal for several cycles.

4. Conclusions

Nowadays, one of the most important sources of environmental pollution is chemical coloring agents in wastewater released from textile factories. Adsorption was used as a cost-effective and efficient, non-toxic technique for the treatment of wastewater. Optimization of the adsorption process was found effective or high removal efficiency at 50 ppm initial dye concentration, low adsorbent dosage of 0.05 g, maximum time of 30–240 min, and 60°C–70°C temperature, at 5 or 6 pH. For all four adsorbent nanocomposites, the equilibrium adsorption data best fitted to Freundlich isotherm model. All nanocomposites (BMUM, BMSS, BMPF, and BMM) fitted well to pseudo-first-order kinetic model. The finding of the present studies suggests that these marble nanocomposites can be used at the commercial level for wastewater treatment.

Acknowledgments

Princess Nourah bint Abdularahman University Researchers Supporting Project number (PNURSP2023R47), Princess Nourah bint Abdularahman University, Riyadh, Saudi Arabia.

References

[1] F.N. Chaudhry, M.F. Malik, Factors affecting water pollution: a review, J. Ecosyst. Ecography, 7 (2017) 1–3.
[2] M.M. Aljohani, S.D. Al-Qahtani, M. Alshareef, M.G. El-Desouky, A.A. El-Bindary, N.M. El-Metwaly, M.A. El-Bindary, Highly efficient adsorption and removal bio-staining dye from industrial wastewater onto mesoporous Ag-MOFs, Process Saf. Environ. Prot., 172 (2023) 395–407.
[3] H.S. Rai, M.S. Bhattacharyya, J. Singh, T.K. Bansal, P. Vats, U.C. Banerjee, Removal of dyes from the effluent of textile and dyestuff manufacturing industry: a review of emerging techniques with reference to biological treatment, Crit. Rev. Env. Sci. Technol., 35 (2005) 219–238.
[4] M. Kahlown, M. Tahir, H. Rasheed, K. Bhatti, Water Quality Status, National Water Quality Monitoring Programme, Fourth Technical ReportPCRWR 5, 2006.
[5] K.R. Ramakrishna, T. Viraraghavan, Dye removal using low cost adsorbents, Water Sci. Technol., 36 (1997) 189–196.
[6] I. Zahoor, A. Mushtaq, Water pollution from agricultural activities: a critical global review, Int. J. Chem. Biochem. Sci., 23 (2023) 164–176.
[7] A. Tariq, A. Mushtaq, Untreated wastewater reasons and causes: a review of most affected areas and cities, Int. J. Chem. Biochem. Sci., 23 (2023) 121–143.
[8] F. Asghar, A. Mushtaq, The future of nanomaterial in wastewater treatment: a review, Int. J. Chem. Biochem. Sci., 23 (2023) 150–157.
[9] A. Choudhary, A. Mushtaq, From pollutant to valuable product: a novel reutilization strategy of wastewater, Int. J. Chem. Biochem. Sci., 23 (2023) 31–37.
[10] T. Fatima, A. Mushtaq, Efficacy and challenges of carbon-based nanomaterials in water treatment: a review, Int. J. Chem. Biochem. Sci., 23 (2023) 232–248.
[11] M.S. Hamada, R.A. Jabal, Doped (Ag) ZnO nanoparticles for removal of azo dyes from aqueous solutions, Int. J. Chem. Biochem. Sci., 21 (2022) 210–217.
[12] A. Javed, A. Mushtaq, A critical review of electrocoagulation and other electrochemical methods, Int. J. Chem. Biochem. Sci., 23 (2023) 98–110.
[13] Z. Rehman, A. Mushtaq, Advancements in treatment of high-salinity wastewater: a critical, Int. J. Chem. Biochem. Sci., 23 (2023) 1–10.
[14] G. Moussavi, M. Mahmoudi, Removal of azo and anthraquinone reactive dyes from industrial wastewaters using MgO nanoparticles, J. Hazard. Mater., 168 (2009) 806–812.
[15] S. Hildenbrand, F. Schmahl, R. Wodarz, R. Kimmel, P. Dartsch, Azo dyes and carcinogenic aromatic amines in cell cultures, Int. Arch. Occup. Environ. Health, 72 (1999) M052–M056.
[16] H.S. Rai, M.S. Bhattacharyya, J. Singh, T. Bansal, P. Vats, U. Banerjee, Removal of dyes from the effluent of textile and dyestuff manufacturing industry: a review of emerging techniques with reference to biological treatment, Crit. Rev. Env. Sci. Technol., 35 (2005) 219–238.
[17] R. Shokoohi, V. Vatanpoor, M. Zarrabi, A. Vatani, Adsorption of Acid Red 18 (AR18) by activated carbon from poplar wood-a kinetic and equilibrium study, E-J. Chem., 7 (2010) 65–72.
[18] S. Khamparia, D.K. Jaspal, Adsorption in combination with ozonation for the treatment of textile waste water: a critical review, Front. Environ. Sci. Eng., 11 (2017) 8, doi: 10.1007/s11783-017-0899-5.
[19] G.A. AlHazmi, K.S. AbouMelha, M.G. El-Desouky, A.A. El-Bindary, Effective adsorption of doxorubicin hydrochloride on zirconium metal-organic framework: equilibrium, kinetic and thermodynamic studies, J. Mol. Struct., 1258 (2022) 132679, doi: 10.1016/j.molstruc.2022.132679.
[20] D. Mohan, K.P. Singh, G. Singh, K. Kumar, Removal of dyes from wastewater using flyash, a low-cost adsorbent, Ind. Eng. Chem., 41 (2002) 3688–3695.
[21] X. Qu, P.J.J. Alvarez, Q. Li, Applications of nanotechnology in water and wastewater treatment, Water Res., 47 (2013) 3931–3946.
[22] M.A. El-Bindary, M.G. El-Desouky, A.A. El-Bindary, Metal–organic frameworks encapsulated with an anticancer compound as drug delivery system: synthesis, characterization, antioxidant, anticancer, antibacterial, and molecular docking investigation, Appl. Organomet. Chem., 36 (2022) e6660, doi: 10.1002/aoc.6660.
[23] A.F. Alkaim, A.M. Ajobree, White marble as an alternative surface for removal of toxic dyes (methylene blue) from aqueous solutions, Int. J. Adv. Sci. Technol., 29 (2020) 5470–5479.
[24] A. Ahmad, S.H. Mohd-Setapar, C.S. Chuong, A. Khatoon, W.A. Wani, R. Kumar, M. Rafatullah, Recent advances in new generation dye removal technologies: novel search for approaches to reprocess wastewater, RSC Adv., 5 (2015) 30801–30818.
[25] P. Assefi, M. Ghaedi, A. Ansari, M. Habibi, M. Momeni, Artificial neural network optimization for removal of hazardous dye Eosin Y from aqueous solution using Co_2O_3-NP-AC: isotherm and kinetics study, J. Ind. Eng. Chem., 20 (2014) 2905–2913.
[26] L. Lendvai, T. Singh, G. Fekete, A. Patnaik, G. Dogossy, Utilization of waste marble dust in poly(lactic acid)-based biocomposites: mechanical, thermal and wear properties, J. Polym. Environ., 29 (2021) 2952–2963.
[27] M.M. Hamed, I. Ahmed, S. Metwally, Adsorptive removal of methylene blue as organic pollutant by marble dust as eco-friendly sorbent, J. Ind. Eng. Chem., 20 (2014) 2370–2377.
[28] Z. Aksu, Application of biosorption for the removal of organic pollutants: a review, Process Biochem., 40 (2005) 997–1026.
[29] G.K. Sarma, A. Khan, A.M. El-Toni, M.H. Rashid, Shape-tunable CuO-Nd$(OH)_3$ nanocomposites with excellent adsorption capacity in organic dye removal and regeneration of spent adsorbent to reduce secondary waste, J. Hazard. Mater., 380 (2019) 120838, doi: 10.1016/j.jhazmat.2019.120838.
[30] D. Suteu, T. Malutan, Industrial cellolignin wastes as adsorbent for removal of methylene blue dye from aqueous solutions, BioRes, 8 (2013) 427–446.
[31] A.-B. Andres, T. Alfredo Campos, O.-M. Mario, Adsorption Isotherms: Enlightenment of the Phenomenon of Adsorption, I. Muharrem, I. Olcay Kaplan, Eds., Wastewater Treatment, IntechOpen, Rijeka, 2022.
[32] N. Lv, X. Wang, Study of the kinetics and equilibrium of the adsorption of oils onto hydrophobic jute fiber modified via the sol-gel method, Int. J. Environ. Res. Public Health, 15 (2018) 969, doi: 10.3390/ijerph15050969.
[33] S. Velusamy, A. Roy, S. Sundaram, T. Kumar Mallick, A review on heavy metal ions and containing dyes removal through graphene oxide-based adsorption strategies for textile wastewater treatment, Chem. Rec., 21 (2021) 1570–1610.
[34] A. Kapałka, G. Fóti, C. Comninellis, Kinetic modelling of the electrochemical mineralization of organic pollutants for wastewater treatment, J. Appl. Electrochem., 38 (2008) 7–16.
[35] Z. Aksu, Biosorption of reactive dyes by dried activated sludge: equilibrium and kinetic modelling, Biochem. Eng. J., 7 (2001) 79–84.
[36] N. Pramanpol, N. Nitayapat, Adsorption of reactive dye by eggshell and its membrane, Kasetsart J. (Nat. Sci.), 40 (2006) 192–197.
[37] S. Mishra, A. Maiti, Study of simultaneous bioremediation of mixed reactive dyes and Cr(VI) containing wastewater through designed experiments, Environ. Monit. Assess., 191 (2019) 1–21.
[38] S. Mishra, P. Mohanty, A. Maiti, Bacterial mediated bio-decolourization of wastewater containing mixed reactive dyes using jack-fruit seed as co-substrate: process optimization, J. Cleaner Prod., 235 (2019) 21–33.

[39] T.W. Leal, L.A. Lourenco, A.S. Scheibe, S.M.G.U. de Souza, A.A.U. de Souza, Textile wastewater treatment using low-cost adsorbent aiming the water reuse in dyeing process, J. Environ. Chem. Eng., 6 (2018) 2705–2712.
[40] B. Rana, J. Chakraborty, Decolourisation of reactive dyes with laccase-mediator system, Res. J. Text. Apparel, 25 (2020) 75–88.
[41] S. Farrokhzadeh, H. Razmi, B. Jannat, Study of Reactive Red 195 anionic dye adsorption on calcined marble powder as potential eco-friendly adsorbent, Human Health Halal Metrics, 1 (2020) 42–56.
[42] S.S. Hassan, N.S. Awwad, A.H. Aboterika, Removal of synthetic reactive dyes from textile wastewater by Sorel's cement, J. Hazard. Mater., 162 (2009) 994–999.
[43] H.A. Kiwaan, F.S. Mohamed, N.A. El-Ghamaz, N.M. Beshry, A.A. El-Bindary, Experimental and electrical studies of Na-X zeolite for the adsorption of different dyes, J. Mol. Liq., 332 (2021) 115877, doi: 10.1016/j.molliq.2021.115877.
[44] H.A. Kiwaan, F. Sh. Mohamed, A.A. El-Bindary, N.A. El-Ghamaz, H.R. Abo-Yassin, M.A. El-Bindary, Synthesis, identification and application of metal organic framework for removal of industrial cationic dyes, J. Mol. Liq., 342 (2021) 117435, doi: 10.1016/j.molliq.2021.117435.
[45] A. Akhtar, M.A. Hanif, U. Rashid, I.A. Bhatti, F.A. Alharthi, E.A. Kazerooni, Advanced treatment of direct dye wastewater using novel composites produced from hoshanar and sunny grey waste, Separation, 9 (2022) 425, doi: 10.3390/separations9120425.
[46] T.A. Altalhi, M.M. Ibrahim, G.A.M. Mersal, M.H.H. Mahmoud, T. Kumeria, M.G. El-Desouky, A.A. El-Bindary, M.A. El-Bindary, Adsorption of doxorubicin hydrochloride onto thermally treated green adsorbent: equilibrium, kinetic and thermodynamic studies, J. Mol. Struct., 1263 (2022) 133160, doi: 10.1016/j.molstruc.2022.133160.